Bioorganic & Medicinal Chemistry 20 (2012) 6375–6383

Contents lists available at SciVerse ScienceDirect

Bioorganic & Medicinal Chemistry

journal homepage: www.elsevier.com/locate/bmc

Design, synthesis and in vitro evaluation of a series of α-substituted phenylpropanoic acid PPARγ agonists to further investigate the stereochemistry–activity relationship

Masao Ohashi [a], Izumi Nakagome [b], Jun-ichi Kasuga [c], Hiromi Nobusada [a], Kenji Matsuno [a], Makoto Makishima [d], Shuichi Hirono [b], Yuichi Hashimoto [c], Hiroyuki Miyachi [a,*]

[a] Graduate School of Medicine, Dentistry and Pharmaceutical Sciences, Okayama University, 1-1-1 Tsushima-Naka, Kita-ku, Okayama 700-8530, Japan
[b] School of Pharmaceutical Sciences, Kitasato University, 5-9-1 Shirokane, Minato-ku, Tokyo 108-8641, Japan
[c] Institute of Molecular and Cellular Biosciences, The University of Tokyo, 1-1-1 Yayoi, Bunkyo-ku, Tokyo 113-0032, Japan
[d] School of Medicine, Nihon University, 30-1 Oyaguchi-kamicho, Itabashi-ku, Tokyo 173-8610, Japan

ARTICLE INFO

Article history:
Received 3 August 2012
Revised 28 August 2012
Accepted 29 August 2012
Available online 11 September 2012

Keywords:
Peroxisome proliferator-activated receptor
PPAR
PPARγ
Phenylpropanoic acid
SAR

ABSTRACT

We previously demonstrated that the α-benzylphenylpropanoic acid-type PPARγ-selective agonist **6** exhibited a reversed stereochemistry–activity relationship, that is, the (*R*)-enantiomer is a more potent PPARγ agonist than the (*S*)-enantiomer, compared with structurally similar α-ethylphenylpropanoic acid-type PPAR agonists. Here, we designed, synthesized and evaluated the optically active α-cyclohexylmethylphenylpropanoic acid derivatives **7** and α-phenethylphenylpropanoic acid derivatives **8**, respectively. Interestingly, α-cyclohexylmethyl derivatives showed reversal of the stereochemistry–activity relationship [i.e., (*R*) more potent than (*S*)], like α-benzyl derivatives, whereas α-phenethyl derivatives showed the 'normal' relationship [(*S*) more potent than (*R*)]. These results suggested that the presence of a branched carbon atom at the β-position with respect to the carboxyl group is a critical determinant of the reversed stereochemistry–activity relationship.

1. Introduction

The peroxisome proliferator-activated receptors (PPARs) are ligand-dependent transcription factors belonging to the nuclear receptor (NR) superfamily; they are activated by endogenous fatty acids and their metabolites, and by synthetic ligands.[1–3] In the presence of a ligand, PPARs heterodimerize with another nuclear receptor, retinoid X receptor (RXR), and the heterodimers modulate transcription of target genes by binding to PPAR response elements in the promoter region of the target genes.[4] The three subtypes (PPARα, PPARδ, and PPARγ) identified to date[5] are differentially expressed in a tissue-specific manner,[6] and play pivotal roles in not only metabolic homeostasis,[7] but also various kinds of biological responses.[8–12] Therefore, PPARs have been recognized as molecular targets for drug development since the 1990s.

We have been interested in structural development of NR ligands (agonists and antagonists) for over 10 years, based on our working hypothesis concerning the NR ligand superfamily,[13] and we have already successfully designed many optically active α-substituted phenylpropanoic acids, including a human PPARα-selective agonist (**1**),[14,15] PPARα/δ dual agonist (**2**, **3**),[16,17] PPARδ-selective agonist (**4**),[18,19] and PPARα/δ/γ pan agonist (**5**) (Fig. 1).[20]

Previous structure–activity relationship (SAR) data on our compounds indicated that the (*S*)-enantiomers are more potent human PPAR transactivators than the antipodal (*R*)-enantiomers, in good agreement with data reported for other series of PPARγ agonists.[21,22] However, we recently found a notable exception. The α-benzylphenylpropanoic acid-type PPARγ-selective agonist, **6** exhibited a reversed stereochemistry–activity relationship, that is, the (*R*)-enantiomer is a more potent hPPARγ agonist than the (*S*)-enantiomer (Table 1).[23] This interesting discrepancy was investigated by means of X-ray crystallographic analysis and computational chemistry based on the obtained X-ray crystallographic data.[23] It was concluded that, although the stereochemistry at the α-position of the carboxyl group is opposite between (*R*)-**6** and (*S*)-**6**, the benzyl side chains of both enantiomers are hosted in the same hydrophobic pocket of hPPARγ LBD, formed by the H3, H5, H7, H11, and H12 helixes (referred to as the benzyl pocket), and in the case of (*S*)-**6**, this involves a short contact between the 2-position hydrogen atom of the benzyl group and the oxygen

Abbreviations: NR, nuclear receptor; hPPAR, human peroxisome proliferator-activated receptor; RXR, retinoid X receptor; LBD, ligand-binding domain; PDB, protein data bank.

* Corresponding author. Tel.: +81 086 251 7930.
E-mail address: miyachi@pharm.okayama-u.ac.jp (H. Miyachi).

0968-0896/$ - see front matter © 2012 Elsevier Ltd. All rights reserved.
http://dx.doi.org/10.1016/j.bmc.2012.08.061

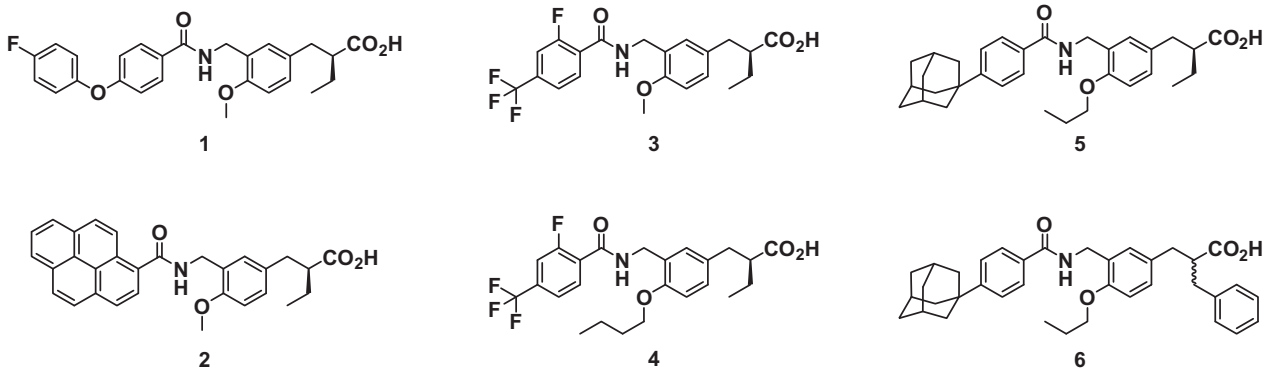

Figure 1. Representatives of our previously developed PPAR agonists. (1) hPPARα-selective agonist. (2,3) hPPARαδ dual agonists. (4) hPPARδ-selective agonist. (5) hPPAR pan agonist. (6) hPPARγ-selective agonist.

Table 1
hPPARs transactivation activities of the present series of α-substituted phenylpropanoic acid derivatives

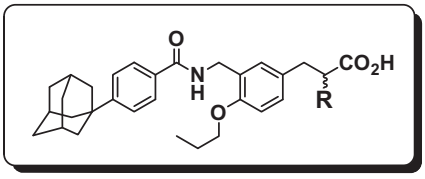

Compd.	R	EC_{50}[a] (nm)		
		hPPARα	hPPARδ	hPPARγ
(*R*)-**6**	Benzyl	ia	ia	3.60 ± 1.1
(*S*)-**6**	Benzyl	ia	ia	22.0 ± 4.0
(*R*)-**7**	Cyclohexylmethyl	ia	ia	13.0 ± 1.6
(*S*)-**7**	Cyclohexylmethyl	ia	ia	22.0 ± 3.0
(*R*)-**5**	Ethyl	500 ± 50	870 ± 70	83.0 ± 10
(*S*)-**5**	Ethyl	54 ± 8	130 ± 40	41.0 ± 9.0
(*R*)-**8**	Phenethyl	1760 ± 83	ia	34.0 ± 2.2
(*S*)-**8**	Phenethyl	770 ± 18	ia	9.2 ± 0.9

[a] Compounds were screened for agonist activity towards PPAR-GAL4 chimeric receptors in transiently transfected HEK-293 cells. The EC_{50} value is the molar concentration of the test compound that affords 50% of the maximal reporter activity.

atom of the side chain of Ser289. Consequently (*S*)-**6** is energetically less stable and somewhat distorted in the complex as compared to (*R*)-**6** (Fig. 2),[23] and this may be the main reason why the (*R*)-enantiomer of **6** exhibits more potent hPPARγ activity than the (*S*)-enantiomer.

Nevertheless, it remained unclear whether a similar situation might hold for other α-substituted phenylpropanoic acids. Therefore, we designed and synthesized a series of novel optically active α-substituted phenylpropanoic acid hPPARγ-selective agonists to further examine the stereochemistry–activity relationship of these compounds.

2. Results and discussion

2.1. Molecular design

First of all, we focused on the structural difference at the β-position with respect to the carboxyl group of **5** and **6**, which exhibited opposite stereochemistry-activity relationships. The introduction of a methyl group at the β-position methylene carbon atom of the carboxyl group afforded the ethyl derivative **5**, which exhibited (*S*)-enantiomer preference. Conversely, introduction of a phenyl group afforded the benzyl derivative **6**, which exhibited the opposite preference. On the basis of this result, we hypothesized that the introduction of ring-structure at the same position might result in reversal of the 'normal' stereochemistry–activity relationship. Accordingly, we designed and synthesized the optically active α-cyclohexylmethylphenypropanoic acids **7** and α-phenethylphenypropanoic acids **8**. The cyclohexylmethyl group was selected to examine the influence of the aromaticity of the benzyl ring of **5**, while the phenethyl group was selected to examine the influence of a branched carbon atom at the β-position (Fig. 3).

2.2. Chemistry

The synthetic route to the desired compounds is shown in Scheme 1. Benzyl 3-bromomethyl benzoate derivative **12**, which was prepared by our previous method,[23] was used as the starting material. It was treated with (*S*)-*N*-3-acyl-4-benzyloxazolidin-2-one according to Evan's asymmetric alkylation protocol,[24] followed by hydrogenolysis to afford benzoic acid derivative **14**. This was reduced with BH_3–THF, then oxidation with PDC afforded the benzaldehyde derivative **12**. This was amide-alkylated with adamantan-1-yl benzamide in the presence of trifluoroacetic acid and triethylsilane as the reducing agent, followed by removal of the chiral auxiliary with LiOOH to afford the desired (*R*)-configuration products (*R*)-**7** and (*R*)-**8** with 98% ee.[25] The antipodal (*S*) enantiomers were similarly prepared from (*R*)-*N*-3-acyl-4-benzyloxazolidin-2-one and showed equivalent optical purity.

2.3. hPPARs transactivation activities of the present series of compounds

To investigate the cell-level hPPARs transactivation activities, we adopted a previously reported hPPARs-responsive reporter gene assay with CMX-GAL4N-hPPARs LBD as the recombinant receptor gene, TK-MH100×4-LUC as the reporter gene and the CMX β-galactosidase gene for normalization.[14] The hPPARs transactivation activities of the new compounds, together with the results for (*R*)-**5**, (*S*)-**5**, (*R*)-**6** and (*S*)-**6**, are summarized in Figures 4 and 5 and Table 1.

As expected, all the enantiomers of α-cyclohexylmethylphenylpropanoic acids **7** and α-phenethylphenylpropanoic acids **8** exhibited potent and selective hPPARγ transactivation activity. These compounds showed about 240-fold and 50-fold selectivity for hPPARγ over the other two hPPAR subtypes, respectively. In addition, as shown in Figure 4, the enantiomers showed the maximum transactivation activities towards hPPARγ at 1 μM concentration,

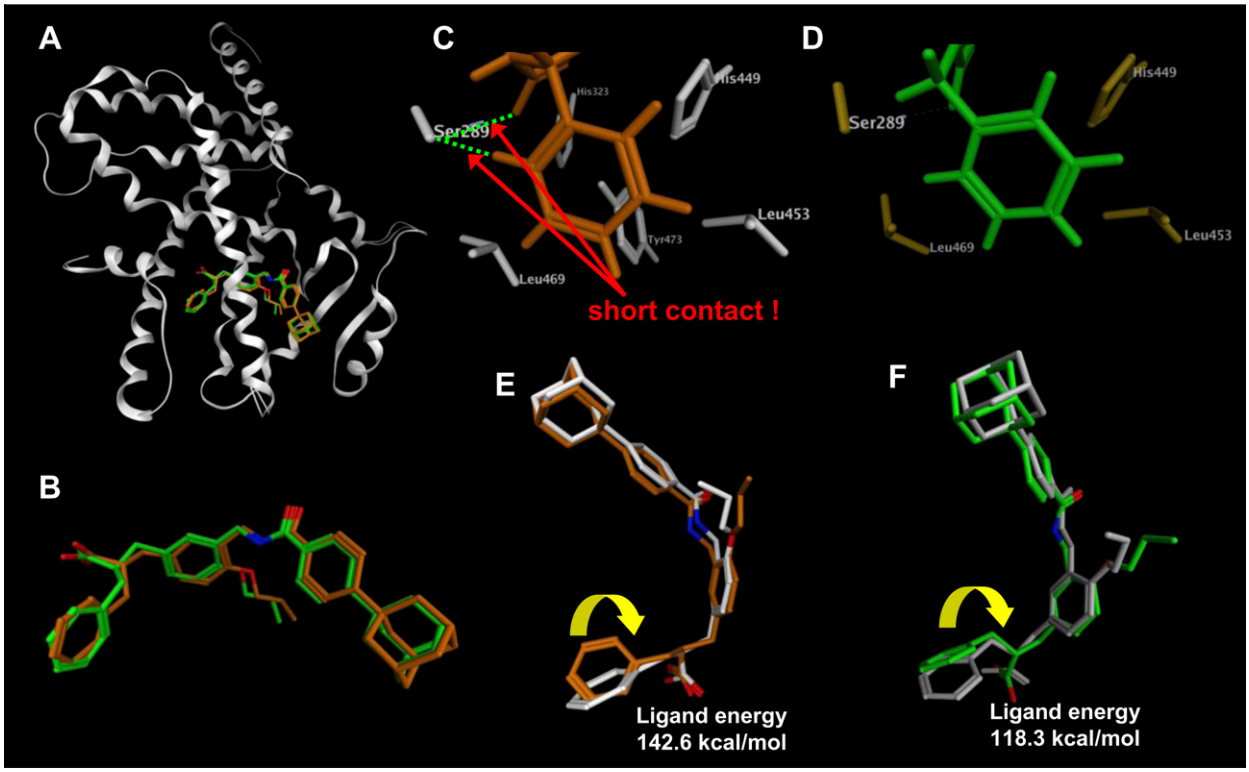

Figure 2. (A) Superposition of the crystal structures of hPPARγ LBD (*S*)-**6** complex and hPPARγ LBD (*R*)-**6** complex. Proteins are represented as wireframe models, and (*S*)-**6** and (*R*)-**6** are depicted as cylinder models in orange ((*S*)-**6** complex) and green ((*R*)-**6** complex). (B) Superposition of the bound structures of (*S*)-**6** and (*R*)-**6**. (C) Zoomed views of the benzyl pocket of hPPARγ LBD (*S*)-**6** complex. (D) Zoomed views of the benzyl pocket of hPPARγ LBD (*R*)-**6** complex. The four interacting amino acids are depicted as white ((*S*)-**6** complex) and yellow cylinders ((*R*)-**6** complex), and the benzyl side chains are depicted in orange ((*S*)-**6**) and green ((*R*)-**6**). (E) Superposition of the bound structure of (*S*)-**6** and the energy-minimized structure of (*S*)-**6**. (F) Superposition of the bound structure of (*R*)-**6** and the energy-minimized structure of (*R*)-**6**. The calculated ligand energies of the bound ligands are shown below the structures. The yellow arrows indicate the directions of distortion of the benzyl groups.

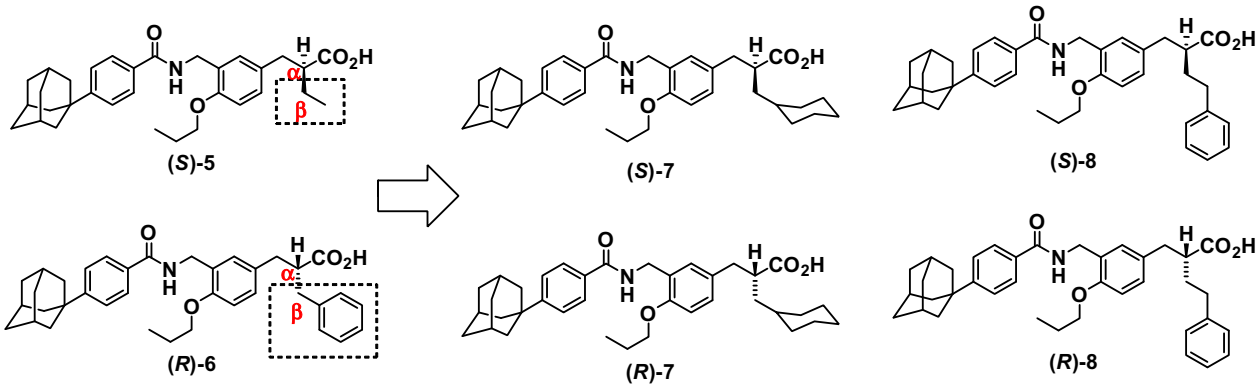

Figure 3. Molecular design of our compounds.

whereas much higher concentrations were needed for apparent activation of the hPPARα and hPPARδ subtypes. These results clearly indicate that the change of the α-position substituent from benzyl to cyclohexylmethyl or phenethyl does not alter the selectivity for hPPARγ, and show that the α-cyclohexylmethylphenylpropanoic acid derivatives **7** and α-phenethylphenylpropanoic acid derivatives **8** are both potent hPPARγ-selective full agonists. The EC_{50} values of these enantiomers for hPPARγ transactivation were somewhat larger to that of (*R*)-**6**, suggesting that the (*R*)-benzyl group has the most favorable hydrophobic interaction with the benzyl pocket among these substituents.

It is of particular interest that (*R*)-**7,** like α-benzylphenylpropanoic acid (*R*)-**6**, exhibited more potent transactivation activity toward PPARγ than did the antipodal (*S*)-**7** (EC_{50} values for hPPARγ were 12.0 and 22.0 nM, respectively). As regards the dose-response relationship, (*R*)-**7** exhibited the maximum transactivation activity at about 50 nM, whereas a much higher concentration of (*S*)-**7** was needed for full activity (Fig. 5). On the other hand, α-phenethylphenylpropanoic acid **8** showed similar SAR to α-ethylphenylpropanoic acid **5**. The EC_{50} values of (*R*)-**8** and (*S*)-**8** for hPPARγ were 34.0 and 9.20 nM, respectively; also, (*S*)-**8** exhibited the maximum transactivation activity at about 50 nM, whereas a much higher concentration of (*R*)-**8** was needed for full activity (Fig. 5).

The observed SAR indicated that the presence of a branched carbon atom at the β-position with respect to the carboxyl group is important for reversal of the stereochemistry–transactivation

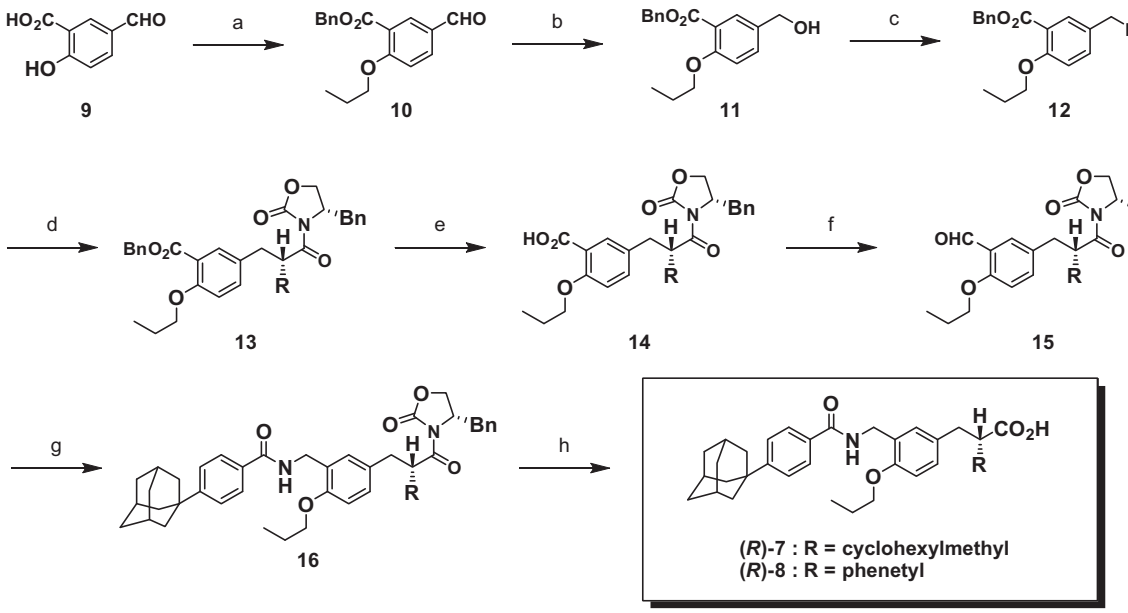

Scheme 1. Synthetic route to the present series of compounds. Reagents and conditions: (a) (1) BnBr, $KHCO_3$, DMF, rt, overnight, 80%, (2) *n*-PrI, K_2CO_3, DMF, 60 °C, 16 h, 91%; (b) $NaBH_4$, EtOH, rt, 2 h, 92%; (c) PBr_3, diethylether, 0 °C, 2 h, 95%; (d) (*S*)-4-benzyl-3-(3-cyclohexylpropanoyl)oxazolidin-2-one or (*S*)-4-benzyl-3-(4- phenylbutanoyl)oxazolidin-2-one, LiHMDS, −50 °C to 0 °C, 2 h, 53–58%; (e) H_2, 10% Pd/C, AcOEt, rt, 2 h, 61–69%; (f) (1) BH_3-THF, THF, 0 °C to rt, overnight, 88–98%, (2) PDC, CH_2Cl_2, rt, overnight, 61–73%; (g) 4-adamantylbenzamide, $(Et)_3SiH$, TFA, toluene, reflux, 48 h, 42–67%; (h) LiOH-H_2O, 30%H_2O_2, THF:H_2O = 4:1 (V/V), 0 °C to rt, 83–86%; (i) (*S*)-4-benzyl-3-(3-cyclohexyl- propanoyl)oxazolidin-2-one or (S)-4-benzyl-3-(4-phenylbutanoyl)oxazolidin-2-one, LiHMDS, −50 °C to 0 °C, 2 h, 50–62%.

activity relationship, rather than the presence of an aromatic ring-containing moiety. For example, in the cases of **6** and **7**, which possess a branched β-carbon, the (*R*)-enantiomers were more potent hPPARγ transactivators than the (*S*)-enantiomers. Conversely, in the case of **5** and **8**, which possess an unbranched β-carbon, the (*S*)-enantiomers were more potent hPPARγ transactivators than the (*R*)-enantiomers. However, the reason for this behavior remained unclear. Therefore, we conducted further studies of the reversal of the stereochemistry–activity relationship in this series by means of computational analysis.

2.4. Construction of the binding model and calculation of the interaction energies

In order to understand the structure-dependent reversal of the stereochemistry–activity relationship, a computational study was performed. First, we constructed binding models of each enantiomer of **7** and **8** with our hPPARγ LBD structure (PDB: 3AN3, 3AN4), using the computational ligand docking program Glide 5.5 in the Schrödinger Suite. Then, we calculated the interaction energies of each enantiomer of **7** and **8** with the hPPARγ LBD. The results are summarized in Figure 6[26] and Table 2. The calculated GlideScores[27,28] were −12.39 and −11.85 for the (*R*)-**7**-hPPARγ LBD complex and (*S*)-**7**-hPPARγ LBD complex, respectively. In the case of **8**, the calculated GlideScores were −12.48 and −12.60 for the (*R*)-**8**- hPPARγ LBD complex and (*S*)-**8**- hPPARγ LBD complex, respectively. Therefore, the (*R*)-**7** complex and the (*S*)-**8** complex were calculated to be more stable than the corresponding enantiomer complexes, in accordance with the finding that (*R*)-**7** and (*S*)-**8** exhibited more potent hPPARγ transactivation activity than their enantiomers. This indicates that glide score is a good predictor of which enantiomer is more stable (potent).

In the case of **7**, the greatest contributor to destabilization of (*S*)-**7**-hPPARγ LBD complex appeared to be Van der Waals energy (evdw). The difference in this hydrophobic parameter indicates that the contribution of the side chains of the amino acids of hPPARγ LBD to the binding is critically different between (*R*)-**7** and (*S*)-**7**. Based on Figure 7, we found that the carbon atom at the α-position of (*S*)-**7** is located very close to Ser289 and Arg288 in the binding region of the hPPARγ LBD that hosts the carboxyl group of the ligand. In the case of (*R*)-**7**, the carbon atom at the α-position of (*R*)-**7** is located in the center of the binding pocket.

On the other hand, none of the energy parameters appears to contribute to destabilization of the (*R*)-**8**-hPPARγ LBD complex as compared to the enantiomeric (*S*)-**8**-hPPARγ LBD complex. However, as mentioned above, we have already reported that distortion of the ligand structure in the form bound to the receptor is an important factor in the reversal of the stereochemistry–activity relationship. For example, the benzyl group of (*S*)-**6** is substantially distorted when (*S*)-**6** is bound to the hPPARγ LBD, that is, the dihedral angle of the bound benzyl group of (*S*)-**6** in the hPPARγ LBD differs by 131° from that of the corresponding energy-minimized structure of (*S*)-**6** itself.[23] Therefore, we examined the distortion of each enantiomer of **8** in the bound form to hPPARγ LBD. These results are summarized in Figure 8. The root-mean-square diameter (rmsd) of (S)-**8** is only 1.04 Å, which indicates that the bound structure of (*S*)-**8** closely resembles the energy-minimized structure. However, in the case of (*R*)-**8**, the rmsd differs by 2.46 Å from that of the energy-minimized structure of (*R*)-**8**.

In conclusion, our results show that the structure of the substituent at the β-position with respect to the carboxyl group in the present series of α-substituted phenylpropanoic acid hPPARγ-selective agonists is critically important in determining the stereochemistry–activity relationship. However, the reasons for the reversal of the stereochemistry–activity relationship might not be precisely the same for the α-cyclohexylmethyl derivative **7** and the phenethyl derivative **8**. An X-ray crystallographic study is in progress to resolve this question.

3. Experimental

3.1. General methods

Melting points were determined with a Yanagimoto hot-stage melting point apparatus and are uncorrected. NMR spectra were recorded on a Varian VNMRS-400 (^{1}H 400 MHz) spectrometer.

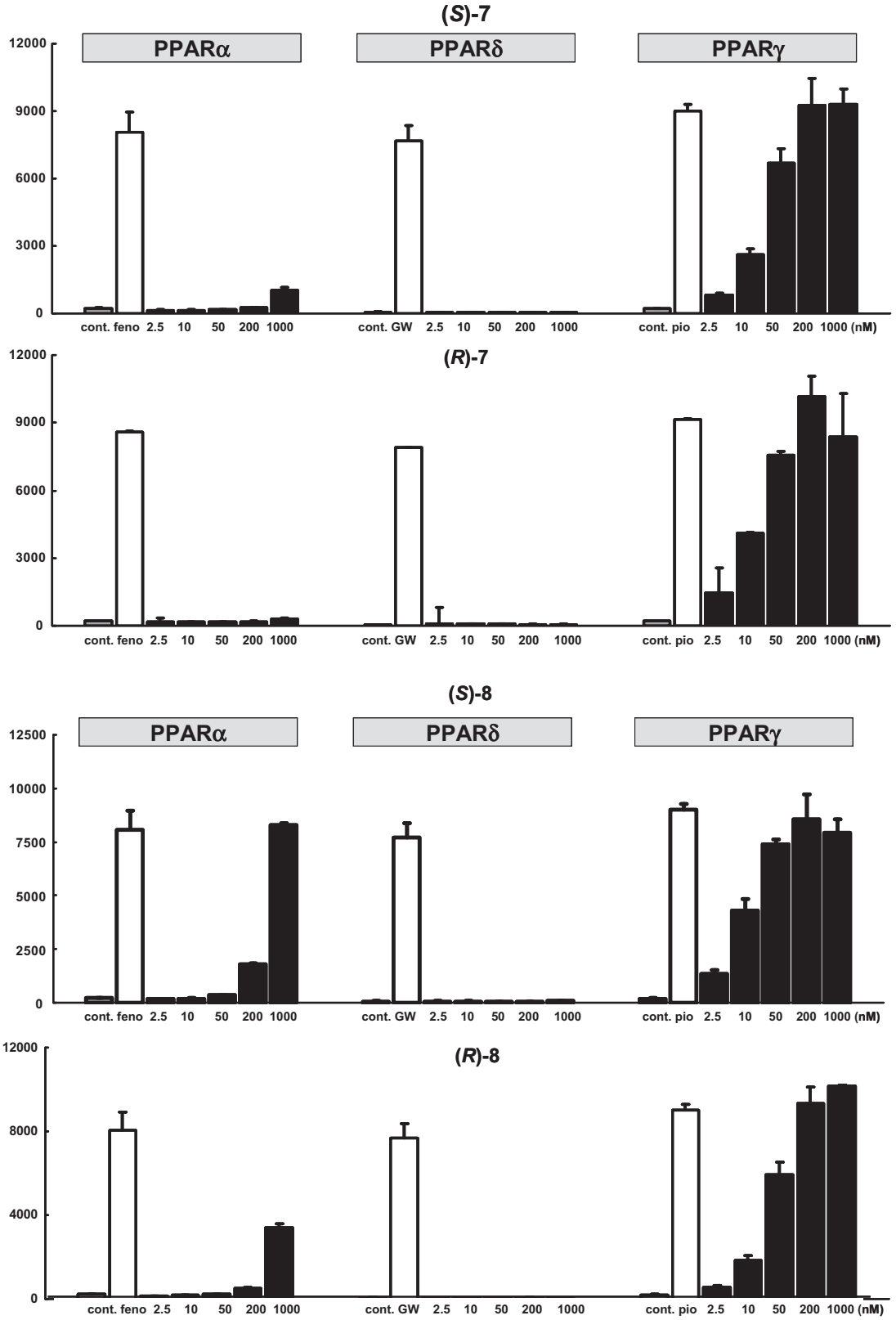

Figure 4. Dose-response relationship of the hPPARs transactivation activities of (*R*)-**7**, (*S*)-**7**, (*R*)-**8** and (*S*)-**8**. Abbreviations used are as follows: feno, 10^{-5} M fenofibrate (PPARα-selective agonist); GW, 10^{-7} M 2-(2-methyl-4-((4-methyl-2-(4-(trifluoromethyl)phenyl)thiazol-5-yl)methylthio)phenyl)acetic acid (GW-501516) (PPARδ-selective agonist); pio, 10^{-6} M pioglitazone (PPARγ-selective agonist).

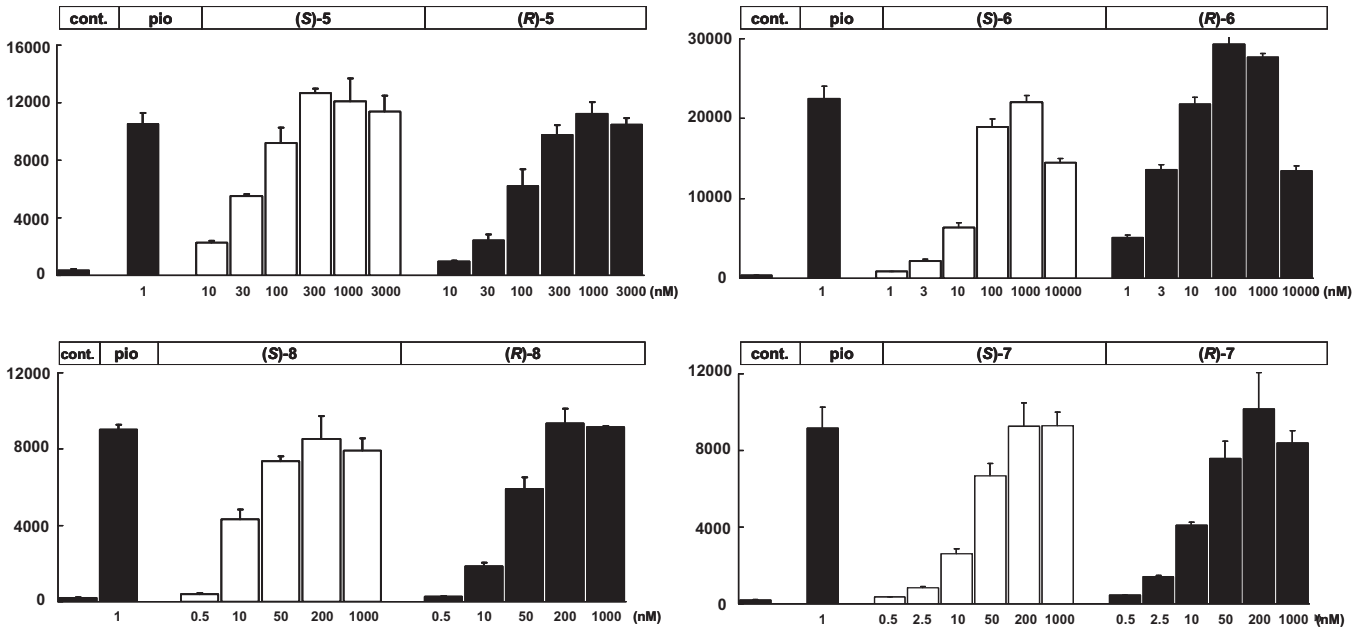

Figure 5. Dose-response relationship of the hPPARγ transactivation activities of both enantiomers of **5**, **6**, **7** and **8.** Abbreviations used are as follows: pio, 10^{-6} M pioglitazone (PPARγ-selective agonist).

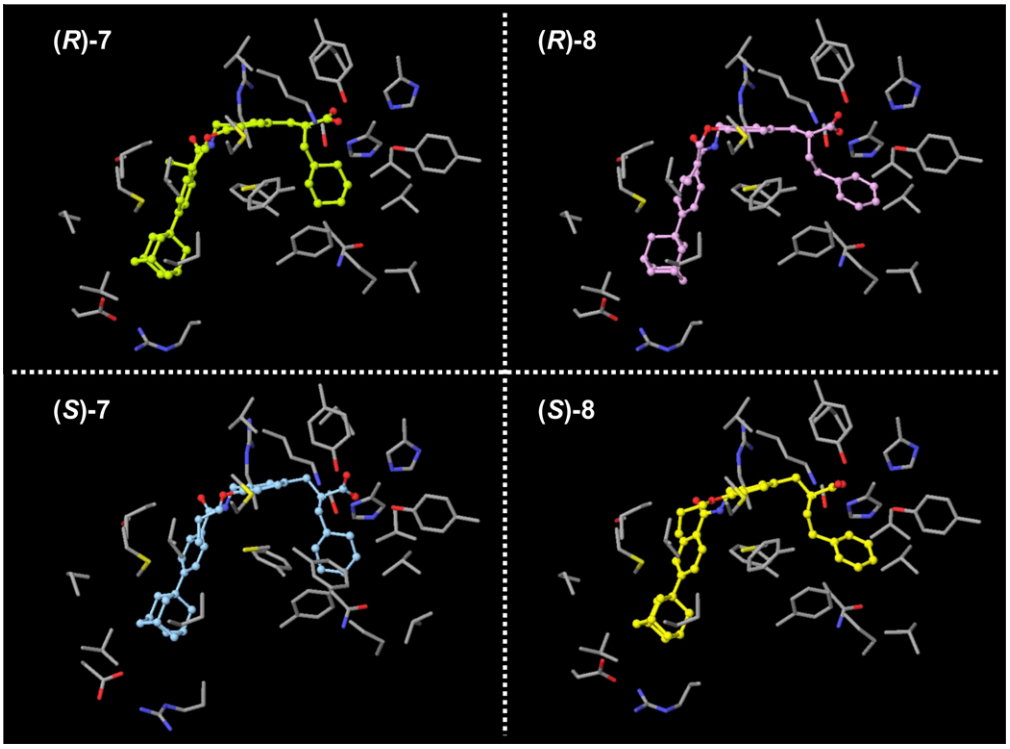

Figure 6. Docking structures of each enantiomer of **7** and **8**, complexed with our hPPARγ LBD structure obtained from the 6-hPPARγ complex (PDB: 3AN3A).

Proton chemical shifts were referenced to TMS internal standard. Elemental analysis was carried out with a Yanagimoto MT-5 CHN recorder elemental analyzer and results were within 0.4% of the theoretical values. FAB-MS was carried out with a VG70-SE.

3.2. Chemistry

3.2.1. Benzyl 5-formyl-2-propoxybenzoate (10)

A mixture of 5-formylsalicylic acid (**8**) (3.00 g, 18.0 mmol), benzyl bromide (2.14 ml, 18.0 mmol), potassium hydrogencarbonate (1.98 g, 19.8 mmol), and 30 mL of *N*,*N*-dimethylformamide was stirred at room temperature for 7 h. The reaction mixture was poured into ice-water and extracted with ethyl acetate. The organic layer was washed with water and brine, dried over anhydrous magnesium sulfate and concentrated. The residue was purified by silica gel column chromatography (eluant; *n*-hexane/ethyl acetate = 7:2 v/v) to afford 3.71 g (80%) as a pale yellow solid. A mixture of this product (3.71 g, 14.5 mmol), iodopropane (2.14 ml, 18.0 mmol), potassium carbonate (2.60 g, 18.9 mmol), and 30 mL of *N*,*N*-dimethylformamide was stirred at 60 °C for 16 h, then

Table 2
Binding energy (GlideScore) calculations for each enantiomer of the phenylpropanoic acid hPPARγ ligands, **7** and **8**. Gscore: GlideScore. Lipo: lipophilic contact plus phobic attractive term in the GlideScore. hbond: hydrogen-bonding term in the GlideScore. Rewards: various reward or penalty terms. evdw: Van der Waals energy. ecoul: Coulomb energy. erotb: penalty for freezing rotatable bonds in the GlideScore

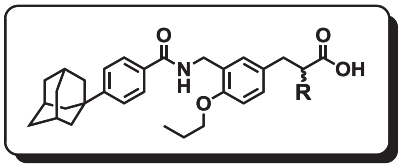

Compd.	R	Glide score	lipo	hbond	Rewards	evdw	ecoul	erotb	Protein
(*R*)-**7**	Cyclohexylmethyl	−12.39	−7.50	−0.29	−0.78	−57.16	−10.10	0.55	3AN3
(*S*)-**7**	Cyclohexylmethyl	−11.85	−6.85	−0.42	−0.56	−54.56	−12.25	0.55	3AN4
(*R*)-**8**	Phenethyl	−12.48	−7.08	−0.38	−0.77	−56.80	−13.22	0.59	3AN3
(*S*)-**8**	Phenethyl	−12.60	−7.81	−0.28	−0.84	−56.32	−9.59	0.59	3AN3

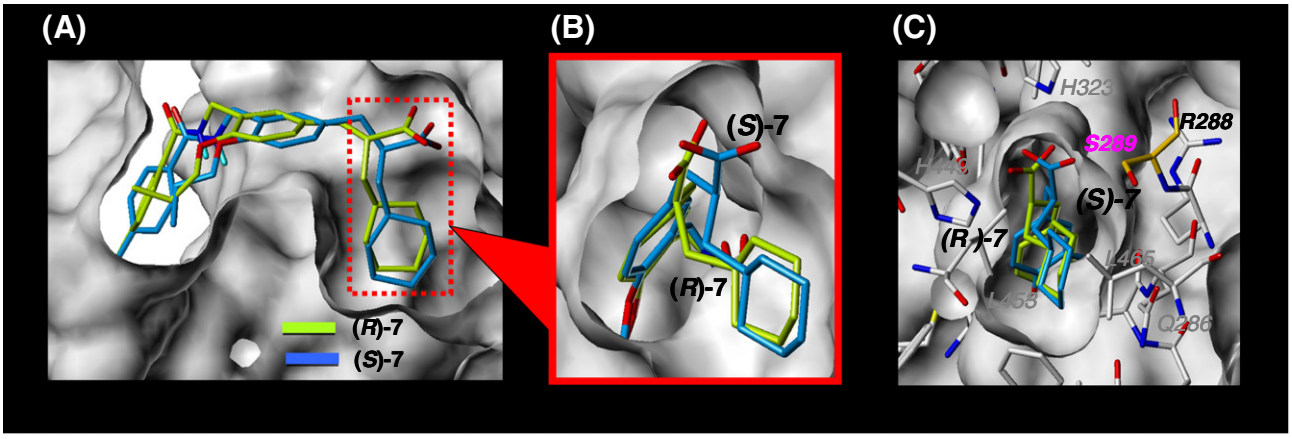

Figure 7. Docking structures of each enantiomer of **7** and **8**, complexed with our hPPARγ LBD structure obtained from 6-hPPARγ complex (PDB: 3AN3A). (a) A Connolly molecular surface map showing the binding poses of (*R*)-**7** and (*S*)-**7** complexed with hPPARγ; (b) and (c) Zoomed view of the binding modes around the cyclohexylmethyl group of **7**.

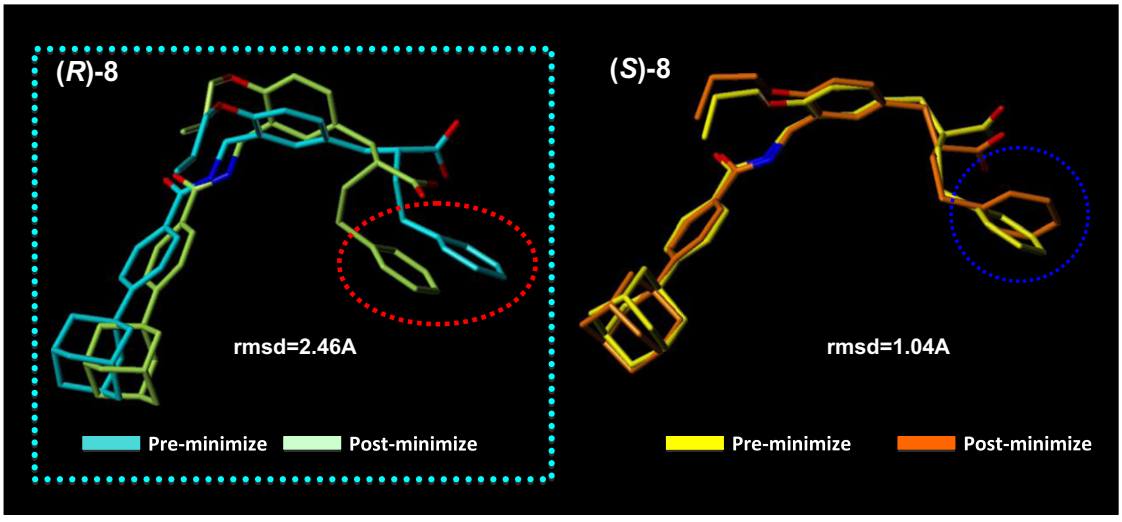

Figure 8. Left: superposition of the bound structure of (*R*)-**8** and the energy-minimized structure of (*R*)-**8**. Right: superposition of the bound structure of (*S*)-**8** and the energy-minimized structure of (*S*)-**8**. The rmsd differences of the bound ligands are indicated.

poured into water and extracted with ethyl acetate. The organic layer was washed with brine, dried over anhydrous magnesium sulfate and concentrated. The residue was purified by silica gel column chromatography (eluant; *n*-hexane/ethyl acetate = 3:1 v/v) to afford 3.90 g (91%) of the title compound as a pale yellow oil. ^{1}H NMR (400 MHz, $CDCl_3$) δ 9.90 (s, 1H), 8.33 (d, J = 2.0 Hz, 1H), 7.99 (dd, J = 8.6, 2.2 Hz, 1H), 7.46 (dd, J = 8.0, 1.2 Hz, 2H), 7.41–7.31 (m, 3H), 7.07 (d, J = 8.8 Hz, 1H), 5.37 (s, 2H), 4.08 (t, J = 6.4 Hz, 2H), 1.89–1.80 (m, 2H), 1.01 (t, J = 7.4 Hz, 3H); MS (FAB) 299 $(M+H)^+$.

3.2.2. Benzyl 5-hydroxymethyl-2-propoxybenzoate (11)

To a solution of **10** (3.90 g, 13.0 mmol) and 30 mL of ethanol was added sodium borohydride (0.50 g, 13.0 mmol) portionwise at 0 °C. The reaction mixture was stirred for 2 h at room temperature. Excess ethanol was evaporated, the residue was poured into water, and the whole was extracted with ethyl acetate. The extract was washed with water and brine, dried over anhydrous magnesium sulfate and concentrated. The residue was purified by silica gel column chromatography (eluant; *n*-hexane/ethyl acetate = 1:1 v/v) to afford 3.58 g (92%) of the title compound as a colorless oil. ^{1}H NMR (400 MHz, $CDCl_3$) δ 7.79 (d, J = 2.4 Hz, 1H), 7.46–7.44 (m, 3H), 7.39–7.31 (m, 3H), 6.94 (d, J = 8.4 Hz, 1H), 5.37 (s, 2H), 4.62 (s, 2H), 3.98 (t, J = 6.4 Hz, 2H), 1.85–1.76 (m, 2H), 0.99 (t, J = 7.4 Hz, 3H); MS (FAB) 301 $(M+H)^+$.

3.2.3. Benzyl 5-bromomethyl-2-propoxybenzoate (12)

A mixture of **11** (3.58 g, 12.0 mmol), phosphorus tribromide (1.13 ml, 12.0 mmol) and 30 mL of dehydrated ether was stirred for 2 h at 0 °C, then poured into ice-water, and the whole was extracted with ether. The extract was washed with water and brine, dried over anhydrous magnesium sulfate and concentrated to afford 4.16 g (95%) of a colorless oil, which was used in the next step without further purification. ^{1}H NMR (400 MHz, $CDCl_3$) δ 7.84 (d, J = 2.4 Hz, 1H), 7.49–7.44 (m, 3H), 7.40–7.31 (m, 3H), 6.92 (d, J = 8.4 Hz, 1H), 5.35 (s, 2H), 4.47 (s, 2H), 3.98 (t, J = 6.4 Hz, 2H), 1.84–1.76 (m, 2H), 0.98 (t, J = 7.4 Hz, 3H).

3.2.4. Benzyl 5-((*R*)-2-benzyl-3-((*S*)-4-benzyl-2-oxo-oxazolidin-3-yl)-3-oxopropyl)-2-propoxybenzoate (13)

(*S*)-4-Benzyl-3-(3-cyclohexylpropanoyl)oxazolidin-2-one (0.75 g, 2.38 mmol) and 10 mL of dehydrated tetrahydrofuran were mixed under an argon atmosphere, and cooled to −50 °C. Under stirring, a 1 mol/L solution of sodium bis(trimethylsilyl)amide in dehydrated tetrahydrofuran (7.20 mL, 7.20 mmol) was added dropwise. After completion of the addition, the mixture was stirred for 1 h at −15 °C and recooled to −50 °C. Then a solution of **12** (1.63 g, 4.49 mmol) in dehydrated tetrahydrofuran (15 mL) was added dropwise to it. After completion of the addition, the mixture was further stirred for 1 h while being gradually heated to room temperature. A saturated aqueous solution of ammonium chloride was added to the reaction mixture, and the whole was extracted with ethyl acetate. The extract was washed with water and brine, dried over anhydrous magnesium sulfate and concentrated. The residue was purified by silica gel column chromatography (eluant; *n*-hexane/ethyl acetate = 15:2 v/v) to afford 0.82 g (58%) of the title compound as a pale yellow oil; MS (FAB) 598 $(M+H)^+$.

3.2.5. 5-((*R*)-3-((*S*)-4-Benzyl-2-oxo-oxazolidin-3-yl)-2-(cyclohexylmethyl)-3-oxopropyl)-2-propoxybenzoic acid (14)

Compound **13** (0.82 g, 1.37 mmol), 10% palladium on carbon (0.17 g) and 30 mL of ethyl acetate were mixed and catalytic hydrogenation was carried out at an initial hydrogen pressure of 200–300 kPa. After completion of the reaction, the catalyst was removed by filtration and the filtrate was concentrated. The residue was purified by silica gel column chromatography (eluant; *n*-hexane/ethyl acetate = 4:1 v/v) to afford 0.48 g (69%) of the title compound as a white solid. ^{1}H NMR (400 MHz, $CDCl_3$) δ 10.99 (s, 1H), 8.03 (dd, J = 2.0 Hz, 1H), 7.54 (dd, J = 8.4, 2.4 Hz, 1H), 7.30–7.22 (m, 3H), 7.10 (dd, J = 8.0, 2.0 Hz, 2H), 6.97 (d, J = 8.4 Hz, 2H), 4.69–4.62 (m, 1H), 4.23–4.15 (m, 5H), 3.16 (dd, J = 13.2, 3.2 Hz, 1H), 3.03 (dd, J = 13.2, 7.2 Hz, 1H), 2.74 (dd, J = 13.4, 7.0 Hz, 1H), 2.55 (dd, J = 13.6, 9.6 Hz, 1H), 1.97–1.88 (m, 2H), 1.76–1.54 (m, 6H), 1.30–1.12 (m, 5H), 1.08 (t, J = 7.4 Hz, 3H), 0.93–0.72 (m, 2H); MS (FAB) 508 $(M+H^+)$.

3.2.6. 5-((*R*)-3-((*S*)-4-Benzyl-2-oxo-oxazolidin-3-yl)-2-(cyclohexylmethyl)-3-oxopropyl)-2-propoxybenzaldehyde (15)

To a solution of **14** (0.48 g, 0.95 mmol) and 30 mL of dehydrated tetrahydrofuran was added dropwise a 1 mol/L solution of borane-tetrahydrofuran complex (1.89 mL, 1.89 mmol). After completion of the addition, the mixture was stirred for 2 h at 0 °C and then overnight at room temperature. A saturated aqueous solution of ammonium chloride was added to the reaction mixture, and the whole was extracted with ethyl acetate. The organic layer was washed with water and brine, dried over anhydrous magnesium sulfate and concentrated. The residue was purified by silica gel column chromatography (eluant; *n*-hexane/ethyl acetate = 3:1 v/v) to afford 0.41 g (88%) of the intermediate hydroxymethyl derivative as a colorless oil. A mixture of the hydroxymethyl derivative (0.41 g, 0.83 mmol), pyridinium dichromate (0.47 g, 1.25 mmol), and 20 mL of dehydrated dichloromethane was stirred for 12 h at room temperature. The catalyst was removed by filtration, and the filtrate was washed with ether and concentrated. The residue was purified by silica gel column chromatography (eluant; *n*-hexane/ethyl acetate = 4:1 v/v) to afford 0.25 g (61%) of the title compound as a white oil. ^{1}H NMR (400 MHz, $CDCl_3$) δ 10.47 (s, 1H), 7.67 (d, J = 2.0 Hz, 1H), 7.50 (dd, J = 8.6, 2,2 Hz, 1H), 7.30–7.23 (m, 3H), 7.09 (dd, J = 7.8, 1.4 Hz, 2H), 6.91 (d, J = 8.8 Hz, 1H), 4.69–4.62 (m, 1H), 4.26–4.07 (m, 3H), 4.04–3.97 (m, 2H), 3.12 (dd, J = 13.2, 3.3 Hz, 1H), 2.99 (dd, J = 13.6, 7.6 Hz, 1H), 2.72 (dd, J = 13.4, 7.0 Hz, 1H), 2.49 (dd, J = 13.2, 10.0 Hz, 1H), 1.92–1.81 (m, 2H), 1.76–1.53 (m, 6H), 1.33–1.10 (m, 5H), 1.05 (t, J = 7.5 Hz, 3H), 0.96–0.75 (m, 2H); MS (FAB) 492 $(M+H^+)$.

3.2.7. 4-(1-Adamantyl)-*N*-((5-((*R*)-3-((*S*)-4-benzyl-2-oxo-oxazolidin-3-yl)-2-(cyclohexylmethyl)-3-oxopropyl)-2-propoxyphenyl)methyl)benzamide (16)

A mixture of **15** (0.25 g, 0.51 mmol), 4-phenylbenzamide (0.39 g, 1.53 mmol), triethylsilane (0.24 mL, 1.53 mmol), trifluoroacetic acid (0.11 mL, 1.53 mmol) and 30 mL of dehydrated toluene was refluxed for 48 h under an argon atmosphere. The reaction mixture was poured into water, and the whole was extracted with ethyl acetate. The extract was washed with water and brine, dried over anhydrous magnesium sulfate and concentrated. The residue was purified by silica gel column chromatography (eluant; *n*-hexane/ethyl acetate = 3:1 v/v) to afford 0.28 g (76%) of the title compound as a pale yellow solid. ^{1}H NMR (400 MHz, $CDCl_3$) δ 7.66 (d, J = 8.8 Hz 2H), 7.36 (d, J = 8.4 Hz, 2H), 7.23–7.18 (m, 4H), 7.15 (d, J = 8.0 Hz, 1H), 6.98 (d, J = 7.6 Hz, 2H), 6.78 (d, J = 8.4 Hz, 1H), 6.59 (t, J = 6.0 Hz, 1H), 4.67–4.57 (m, 3H), 4.33–4.26 (m, 1H), 4.11 (t, J = 7.2 Hz, 1H), 4.03 (d, J = 6.4 Hz, 1H), 3.98–3.89 (m, 2H), 3.02-2.89 (m, 2H), 2.73 (dd, J = 13.2, 6.6 Hz, 1H), 2.39 (dd, J = 13.5, 9.8 Hz, 1H), 2.10 (s, 3H), 1.90–1.53 (m, 20H), 1.37–1.10 (m, 5H), 1.04 (t, J = 7.35 Hz, 3H), 0.94–0.76 (m, 2H); MS (FAB) 731 $(M+H^+)$.

3.2.8. (*R*)-2-((3-(((4-(1-Adamantyl)benzoyl)amino)methyl)-4-propoxyphenyl)methyl)-3-cyclohexylpropanoic acid ((*R*)-7)

Compound **16** (170 mg, 0.38 mmol) was dissolved in 24 mL of tetrahydrofuran and 5 mL of water under an argon atmosphere with ice-cooling. To this solution was added 30% aqueous hydrogen peroxide (0.43 mL, 3.80 mmol). Then a solution of lithium hydroxide monohydrate (64.0 mg, 1.53 mmol) in water (1 mL) was added to it, and the mixture was stirred for 2.5 h at 0 °C and for 3 h at room temperature. An aqueous solution of sodium sulfite (1.00 g/6 mL) was added to the mixture and the whole was stirred further for 15 min. The reaction mixture was acidified with 10% HCl, and then extracted with ethyl acetate. The extract was washed with brine, dried over anhydrous magnesium sulfate and concentrated. The residue was purified by silica gel column chromatography (eluant; *n*-hexane/ethyl acetate = 3:1 v/v) to afford 110 mg (83%) of the title compound as a white crystalline solid; mp

177–178 °C. ^{1}H NMR (300 MHz, $CDCl_3$) δ 7.70 (d, J = 8.4 Hz, 2H), 7.39 (d, J = 8.4 Hz, 2H), 7.14 (s, 1H), 7.04 (dd, J = 8.4, 2.1 Hz, 1H), 6.78–6.70 (m, 2H), 4.65–4.53 (m, 2H), 3.95 (t, J = 6.5 Hz, 2H), 2.87–2.64 (m, 3H), 2.10 (s, 3H), 1.90–1.54 (m, 20H), 1.34–1.12 (m, 5H), 1.06 (t, J = 7.4 Hz, 3H), 0.92–0.73 (m, 2H); HRMS (FAB, MH^+) calcd for $C_{37}H_{50}NO_4$ 572,3740, found 572.3719; $[\alpha]_D$ −5.5° (c 0.50, $CHCl_3$); Anal. ($C_{37}H_{50}NO_4-{}^1/_4H_2O$) C, H, N.

3.2.9. (*S*)-2-((3-(((4-(1-Adamantyl)benzoyl)amino)methyl)-4-propoxyphenyl)methyl)-3-cyclohexylpropanoic acid ((*S*)-7)

This compound was prepared by means of a procedure similar to that used for (*R*)-**7**; mp 177–178 °C; ^{1}H NMR (300 MHz, $CDCl_3$) δ 7.70 (d, J = 8.4 Hz, 2H), 7.39 (d, J = 8.4 Hz, 2H), 7.14 (s, 1H), 7.04 (dd, J = 8.4, 2.1 Hz, 1H), 6.78–6.70 (m, 2H), 4.65–4.53 (m, 2H), 3.95 (t, J = 6.5 Hz, 2H), 2.87–2.64 (m, 3H), 2.10 (s, 3H), 1.90–1.54 (m, 20H), 1.34–1.12 (m, 5H), 1.06 (t, J = 7.4 Hz, 3H), 0.92–0.73 (m, 2H); HRMS (FAB, MH^+) calcd for $C_{37}H_{50}NO_4$ 572,3740, found 572.3735; $[\alpha]_D$ +5.5° (c 0.50, $CHCl_3$); Anal. ($C_{37}H_{50}NO_4$) C, H, N.

3.2.10. (*R*)-2-((3-(((4-(1-Adamantyl)benzoyl)amino)methyl)-4-propoxyphenyl)methyl)-4-phenylbutanoic acid ((*R*)-8)

This compound was prepared by means of a procedure similar to that used for (*R*)-**7**; mp 140–141 °C; ^{1}H NMR (300 MHz, $CDCl_3$) δ 7.69 (d, J = 8.4 Hz, 2H), 7.39 (d, J = 8.1 Hz, 2H), 7.26–7.13 (m, 6H), 7.02 (dd, J = 8.4, 2.1 Hz, 1H), 6.76–6.69 (m, 2H), 4.59 (d, J = 4.5 Hz, 2H), 3.93 (t, J = 6.5 Hz, 2H), 2.91 (dd, J = 13.1, 7.7 Hz, 1H), 2.77–2.53 (m, 4H), 2.10 (s, 3H), 2.04–1.72 (m, 17H), 1.05 (t, J = 7.4 Hz, 3H); HRMS (FAB, MH^+) calcd for $C_{37}H_{50}NO_4$ 580,3427, found 580.3432; $[\alpha]_D$+4° (c 0.25, $CHCl_3$).

3.2.11. (*S*)-2-((3-(((4-(1-Adamantyl)benzoyl)amino)methyl)-4-propoxyphenyl)methyl)-4-phenylbutanoic acid ((*S*)-8)

This compound was prepared by means of a procedure similar to that used for (*R*)-**7**; mp 140–141 °C; ^{1}H NMR (300 MHz, $CDCl_3$) δ 7.69 (d, J = 8.4 Hz, 2H), 7.39 (d, J = 8.1 Hz, 2H), 7.26–7.13 (m, 6H), 7.02 (dd, J = 8.4, 2.1 Hz, 1H), 6.76-6.69 (m, 2H), 4.59 (d, J = 4.5 Hz, 2H), 3.93 (t, J = 6.5 Hz, 2H), 2.91 (dd, J = 13.1, 7.7 Hz, 1H), 2.77–2.53 (m, 4H), 2.10 (s, 3H), 2.04–1.72 (m, 17H), 1.05 (t, J = 7.4 Hz, 3H); HRMS (FAB, MH^+) calcd for $C_{37}H_{50}NO_4$ 580,3427, found 580.3432; $[\alpha]_D$−4° (c 0.25, $CHCl_3$).

3.3. Reporter gene assay

Human embryonic kidney HEK293 cells were cultured in DMEM containing 5% fetal bovine serum and antibiotic-antimycotic mixture (Nacalai) at 37 °C in a humidified atmosphere of 5% CO_2 in air. Transfections were performed by calcium phosphate coprecipitation. Eight hours after transfection, ligands were added. Cells were harvested approximately 16–20 h after the treatment, and luciferase and β-galactosidase activities were assayed using a luminometer and a microplate reader. DNA cotransfection experiments included 50 ng of reporter plasmid, 20 ng pCMX-β-galactosidase, 15 ng each receptor expression plasmid, and pGEM carrier DNA to make a total of 150 ng of DNA per well in a 96-well plate. Luciferase data were normalized to an internal β-galactosidase control and reported values are means of triplicate assays.

3.4. Computational ligand docking

Optically active **7** and **8** were docked into the hPPARγ ligand binding domains (LBDs) (PDB code: 3AN3 and 3AN4) with standard precision mode for Glide 5.5 in the Schrödinger Suite. The GlideScore, which represents the ligand-receptor interaction energy, was calculated for each generated pose. The pose with the best GlideScore was selected as the binding structure of **7** (or **8**) to hPPARγ LBD. In prior to the study, we validated the above docking procedure using the complexed structures of TIPP703, (*S*)-**6** or (*R*)-**6** with the hPPARγ LBDs (PDB code 2ZNO, 3AN3 and 3AN4) determined by X-ray crystallography. In the validation step, we also checked the orientation of the side chain of Phe363 of the hPPARγ LBDs because Phe363 interacts with the R group of the ligand and the orientation of the side chain of Phe363 is different between the X-ray structures bound ligands. In results, we succeeded in reproducing the correct docking structures (to less than 2 Å of the X-ray structures) of TIPP703, (*S*)-**6** and (*R*)-**6** and reproducing the orientation of side chain of Phe363 of the hPPARγ LBDs.

Acknowledgment

This work was supported in part by the Targeted Proteins Research Program of the Japan Science and Technology Corporation (JST), the Uehara Memorial Foundation, the Tokyo Biochemical Research Foundation (TBRF), and the Okayama Foundation for Science and Technology (OFST).

References and notes

1. Desvergne, B.; Wahli, W. *Endocr. Rev.* **1999**, *20*, 649.
2. Dreyer, C.; Krey, G.; Keller, H.; Givel, F.; Helftenbein, G.; Wahli, W. *Cell* **1992**, *68*, 879.
3. Issemann, I.; Green, S. *Nature* **1990**, *347*, 645.
4. Bardot, O.; Aldridge, T. C.; Latruffe, N.; Green, S. *Biochem. Biophys. Res. Commun.* **1993**, *192*, 37.
5. Nuclear Receptors Nomenclature Committee. *Cell* **1999**, *97*, 1.
6. Wahli, W. *Swiss. Med. Wkly.* **2002**, *132*, 83.
7. Mendez, M.; LaPointe, M. C. *Hypertension* **2003**, *42*, 844.
8. Morrison, R. F.; Farmer, S. R. *J. Biol. Chem.* **1999**, *274*, 17088.
9. Huang, J. W.; Shiau, C. W.; Yang, J.; Wang, D. S.; Chiu, H. C.; Chen, C. Y.; Chen, C. S. *J. Med. Chem.* **2006**, *49*, 4684.
10. Wang, N.; Yin, R.; Liu, Y.; Mao, G.; Xi, F. *Circ. J.* **2011**, *75*, 528.
11. Kaundal, R. K.; Sharma, S. S. *Drug News Perspect.* **2010**, *23*, 241.
12. Landreth, G. *Curr. Alzheimer Res.* **2007**, *4*, 159.
13. Hashimoto, Y.; Miyachi, H. *Bioorg. Med. Chem.* **2005**, *13*, 5080.
14. Ban, S.; Kasuga, J.; Nakagome, I.; Nobusada, H.; Takayama, F.; Hirono, S.; Kawasaki, H.; Hashimoto, Y.; Miyachi, H. *Bioorg. Med. Chem.* **2011**, *19*, 3183.
15. Nomura, M.; Tanase, T.; Ide, T.; Tsunoda, M.; Suzuki, M.; Uchiki, H.; Murakami, K.; Miyachi, H. *J. Med. Chem.* **2003**, *46*, 3581.
16. Kasuga, J.; Yamasaki, D.; Araya, Y.; Nakagawa, A.; Makishima, M.; Doi, T.; Hashimoto, Y.; Miyachi, H. *Bioorg. Med. Chem.* **2006**, *14*, 8405.
17. Araya, Y.; Kasuga, J.; Toyota, K.; Hirakawa, Y.; Oyama, T.; Makishima, M.; Morikawa, K.; Hashimoto, Y.; Miyachi, H. *Chem. Pharm. Bull.* **2008**, *56*, 1357.
18. Kasuga, J.; Nakagome, I.; Aoyama, A.; Sako, K.; Ishizawa, M.; Ogura, M.; Makishima, M.; Hirono, S.; Hashimoto, Y.; Miyachi, H. *Bioorg. Med. Chem.* **2007**, *15*, 5177.
19. Kasuga, J.; Oyama, T.; Nakagome, I.; Makishima, M.; Hirono, S.; Morikawa, K.; Hashimoto, Y.; Miyachi, H. *ChemMedChem* **2008**, *3*, 1662.
20. Kasuga, J.; Yamasaki, D.; Ogura, K.; Shimizu, M.; Sato, M.; Makishima, M.; Doi, T.; Hashimoto, Y.; Miyachi, H. *Bioorg. Med. Chem. Lett.* **2008**, *18*, 1110.
21. Cobb, J. E.; Blanchard, S. G.; Boswell, E. G.; Brown, K. K.; Charifson, P. S.; Cooper, J. P.; Collins, J. L.; Dezube, M.; Henke, B. R.; Hull-Ryde, E. A.; Lake, D. H.; Lenhard, J. M.; Oliver, W., Jr.; Oplinger, J.; Pentti, M.; Parks, D. J.; Plunket, K. D.; Tong, W. Q. *J. Med. Chem.* **1998**, *41*, 5055.
22. Hulin, B.; Newton, L. S.; Lewis, D. M.; Genereux, P. E.; Gibbs, E. M.; Clark, D. A. *J. Med. Chem.* **1996**, *39*, 3897.
23. Ohashi, M.; Oyama, T.; Nakagome, I.; Sato, M.; Nishio, Y.; Nobusada, H.; Hirono, S.; Morikawa, K.; Hashimoto, Y.; Miyachi, H. *J. Med. Chem.* **2011**, *54*, 331.
24. Evans, D. A.; Ennis, M. D.; Mathre, D. J. *J. Am. Chem. Soc.* **1982**, *104*, 1737.
25. The enantiomeric excess was determined with a CHIRALPAK AD-H column, with hexane/*i*-PrOH/trifluoroacetic acid = 90:10:0.1 v/v/v as the mobile phase, at a flow rate of 0.5 mL/min, with detection at 254 nm.
26. Computer-graphic work and measurement of hydrogen bonding distances were performed using MOE (Molecular Operating Environment) (Ryoka Systems Inc.).
27. Friesner, R. A.; Banks, J. L.; Murphy, R. B.; Halgren, T. A.; Klicic, J. J. *J. Med. Chem.* **2004**, *47*, 1739.
28. Friesner, R. A.; Murphy, R. B.; Repasky, M. P.; Frye, L. L.; Greenwood, J. R. *J. Med. Chem.* **2006**, *49*, 6177.